Crystalline Oligo(ethylene sulfide) Domains Define Highly Stable Supramolecular Block Copolymer Assemblies

Carrie E. Brubaker,[†] Diana Velluto,[†,#] Davide Demurtas,[‡] Edward A. Phelps,[†] and Jeffrey A. Hubbell[*,†,§,∥,⊥]

[†]Institute of Bioengineering, School of Life Sciences, [‡]Interdisciplinary Centre for Electron Microscopy, and [§]Institute of Chemical Sciences and Engineering, School of Basic Sciences, Ecole Polytechnique Fédérale de Lausanne, 1015 Lausanne, Switzerland, [∥]Institute for Molecular Engineering, University of Chicago, Chicago, Illinois 60637, United States, and [⊥]Materials Science Division, Argonne National Laboratory, Argonne, Illinois 60439, United States. [#]Present address: Diabetes Research Institute, University of Miami, Miami, Florida 33136, United States.

ABSTRACT With proper control over copolymer design and solvation conditions, self-assembled materials display impressive morphological variety that encompasses nanoscale colloids as well as bulk three-dimensional architectures. Here we take advantage of both hydrophobicity and crystallinity to mediate supramolecular self-assembly of spherical micellar, linear fibrillar, or hydrogel structures by a family of highly asymmetric poly(ethylene glycol)-*b*-oligo(ethylene sulfide) (PEG-OES) copolymers. Assembly structural polymorphism was achieved with modification of PEG-OES topology (linear versus multiarm) and with precise, monomer-by-monomer control of OES length. Notably, all three morphologies were accessed utilizing OES oligomers with degrees of polymerization as short as three. These exceptionally small assembly forming blocks represent the first application of ethylene sulfide oligomers in supramolecular materials. While the assemblies demonstrated robust aqueous stability over time, oxidation by hydrogen peroxide progressively converted ethylene sulfide residues to increasingly hydrophilic and amorphous sulfoxides and sulfones, causing morphological changes and permanent disassembly. We utilized complementary microscopic and spectroscopic techniques to confirm this chemical stimulus-responsive behavior in self-assembled PEG-OES colloidal dispersions and physical gels. In addition to inherent stimulus-responsive behavior, fibrillar assemblies demonstrated biologically relevant molecular delivery, as confirmed by the dose-dependent activation of murine bone marrow-derived dendritic cells following fibril-mediated delivery of the immunological adjuvant monophosphoryl lipid A. In physical gels composed of either linear or multiarm PEG-OES precursors, rheologic analysis also identified mechanical stimulus-responsive shear thinning behavior. Thanks to the facile preparation, user-defined morphology, aqueous stability, carrier functionality, and stimuli-responsive behaviors of PEG-OES supramolecular assemblies, our findings support a future role for these materials as injectable or implantable biomaterials.

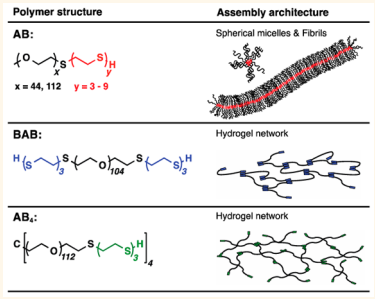

KEYWORDS: polymer · self-assembly · nanoparticle · micelle · cylindrical micelle · hydrogel

One of the hallmarks of polymer-based supramolecular self-assembly is structural polymorphism, achieved by rational design of assembly forming species within a complex, multiparameter space.[1,2] The same factors that control assembly morphology may also influence assembly kinetics, downstream functionality, and disassembly mechanisms, which subsequently impact the use of hierarchical assemblies as applied materials.[3,4] Spherical morphologies are most commonly explored, and while these copolymer-derived micellar and vesicular structures are widely utilized, wormlike micelles and other filamentous, high aspect ratio assemblies have garnered increased attention as molecular delivery platforms thanks to enhanced, controllable loading capacities,[5,6] extended *in vivo* blood circulation behaviors,[7] and improved understanding of the role of anisotropy in cellular internalization and tissue targeting.[8,9] Advanced microscopic[10] and spectroscopic[11] techniques have further characterized fibrillar structural dynamics. For such applications, the amphiphilic block copolymer constituents of self-assembled fibrillar colloidal materials are designed to yield these architectures specifically. Taking an alternative approach, controlled modulation of copolymer structural parameters such as block size and number has permitted

* Address correspondence to jeffrey.hubbell@epfl.ch or jhubbell@uchicago.edu.

Received for review January 13, 2015 and accepted June 30, 2015.

Published online June 30, 2015
10.1021/acsnano.5b02937

systematic exploration of self-assembly polymorphism, yielding spherical, fibrillar/worm-like, and (multi)-lamellar structures.[12−14] Here we extend the approach, employing a family of highly asymmetric block copolymers to generate spherical and fibrillar colloidal assemblies, as well as three-dimensional network structures.

The majority of polymer-based self-assembled materials are derived from amorphous or semicrystalline amphiphiles, and assembly is commonly driven by hydrophobic or electrostatic interactions, hydrogen bonding, $\pi-\pi$ stacking, or combinations thereof.[15,16] Expanding from these mechanisms, interest has recently focused on mediating self-assembly via crystallinity of assembly forming domain(s). Taking advantage of the technique known as "crystallization-driven self-assembly," spherical micelles, cylindrical (fibrillar) micelles, comicelles, platelets, and scarf-like structures have been accessed by poly(ferrocenylsilane)-containing copolymers.[17−19] Structural polymorphism has also been explored in copolymer assemblies defined by the crystallization of poly(ε-caprolactone),[20] poly(lactide),[21] poly(ethylene),[22] and poly(ethylene oxide)[23] domains. A recent review has highlighted the ability of crystallization mechanisms to precisely control assembly of cylindrical micelles in particular.[24] Taking inspiration from these findings, we sought to develop a copolymer self-assembly platform employing very small crystalline domains as assembly forming blocks and drivers of structural polymorphism.

The crystalline structure of poly(ethylene sulfide) has been known,[25] with refinements,[26] for decades. Previous attempts[27] to incorporate poly(ethylene sulfide) into block copolymer materials met with distinct disadvantages: the polymers were insoluble in all common solvents, and processing temperatures approached those established for ethylene sulfide thermal degradation. Nevertheless, low molecular weight ethylene sulfide blocks within these materials were found to be crystalline.[27] Re-examining a functional role for ethylene sulfide domains in polymeric materials, we utilize a synthetic strategy that overcomes these limitations, benefiting from very low degrees of ethylene sulfide polymerization to maintain block copolymer solubility, to provide very small assembly forming blocks, and to define assembly morphology. There is precedent for exploiting very small, assembly forming blocks in supramolecular materials; for example, a family of bisurea-poly(ethylene glycols) are known to form rodlike micelles[28] as well as hydrogels,[29] through hydrogen bonding of their small, hydrophobic bisurea domains.

In addition to modulating assembly morphology, copolymer chemistry defines stimulus-responsive behaviors and/or disassembly mechanisms of supramolecular structures. A spectrum of defined control exists

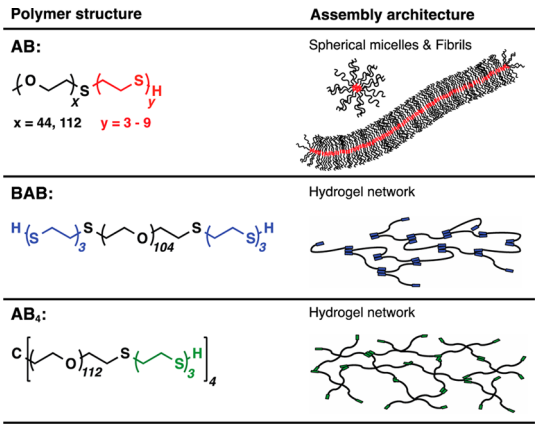

Figure 1. AB diblock, BAB triblock, and AB_4 multiarm copolymer amphiphiles based on poly(ethylene glycol)-*b*-oligo(ethylene sulfide) (PEG-OES) form supramolecular self-assemblies. In these colloidal and three-dimensional network materials, PEG-OES block size and topology inform structural morphology. Structural representations are for visual description and are not to scale.

which includes relatively nonspecific hydrolytic susceptibility, thermal or light sensitivity, highly specific conformal or enzymatic reactivity, and biologically relevant pH or redox dependence. In particular, we may take advantage of oxidation-responsive behavior to design self-assembled materials that respond, disassemble, or degrade in the context of extracellular inflammation or intracellular postphagocytic lysosomal processing.[30] Previous efforts in our group have characterized oxidation-mediated morphological changes of polymersome vesicles[31] in which poly(propylene sulfide) represented the assembly forming domain. In micelles produced by electrostatic interactions between a cationic selenium-containing surfactant and poly(ethylene glycol)-*b*-poly(acrylic acid), sensitivity of the selenide group to oxidation led to micellar disassembly.[32] Following self-assembly of tetrathiafulvalene-functionalized ethylene glycol-based amphiphiles, disruption of the micellar structures occurred upon treatment with oxidative iron(III) perchlorate $Fe(ClO_4)_3$.[33] In these materials, copolymer chemistry defines their oxidation sensitivity, thereby defining a stimulus-responsive behavior manifested by disassembly of the supramolecular structures. Such disassembly mechanisms are particularly desirable in the context of downstream biological applications, where oxidation-sensitive materials are exposed to extracellular or postphagocytic intracellular conditions that permit nontoxic clearance from the organism as single polymer species.[34]

We introduce a family of highly asymmetric coil-crystalline block copolymers capable of forming both colloidal and network assemblies (Figure 1). By first demonstrating synthesis and self-assembly of AB-type poly(ethylene glycol)-*b*-oligo(ethylene sulfide) (PEG-OES) copolymers, we report the dependence of assembly formation and architecture on very short OES

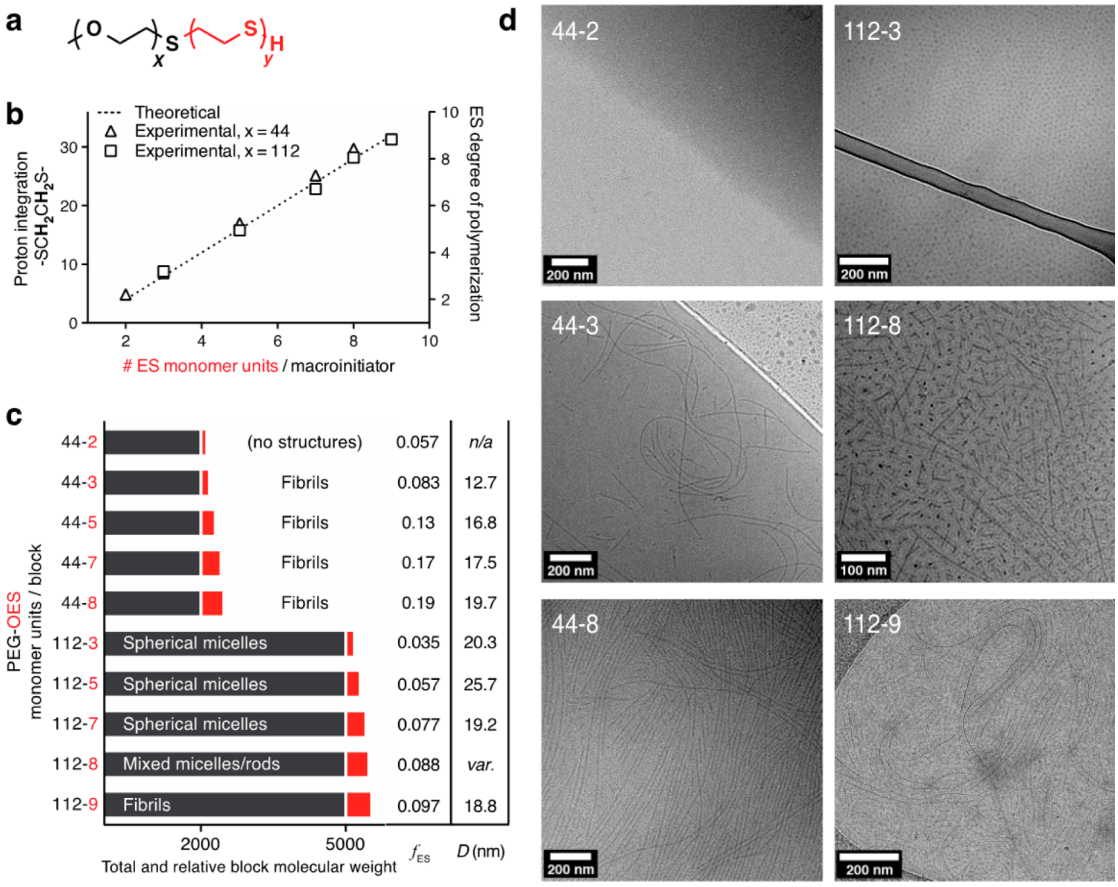

Figure 2. Mass fraction of very short ethylene sulfide (ES) oligomers dictates colloidal self-assembly morphology. (a) General structure of poly(ethylene glycol)-*b*-oligo(ethylene sulfide) (PEG-OES). (b) ES ring-opening polymerization from PEG macroinitiator permits controlled and incremental increase in OES length. The number of feed ES monomers per macroinitiator species is directly reflected in ^{1}H NMR signal integration of sulfur-adjacent protons following OES chain growth, and matches the degree of ES polymerization. (c) By varying the length of PEG and OES blocks, and thus ES mass fraction f_{ES}, spherical micellar, linear fibrillar, or intermediate populations are obtained. (d) Selected electron microscopy of assemblies derived from the indicated PEG-OES diblock copolymer precursors. All samples except 44-2, cryogenic transmission electron microscopy. Sample 44-2 was analyzed by negative stain transmission electron microscopy to confirm absence of assembled species. For complete structural library, see also Supporting Information Figure S3.

segments, the lengths of which differ by as little as one mer. High aspect ratio linear fibrillar assemblies undergo oxidation-mediated shortening yet maintain structural integrity upon long-term storage in water. Fibrillar assemblies act as molecular delivery platforms, facilitating the activation of murine bone marrow-derived dendritic cells by monophosphoryl lipid A (MPLA), an amphiphilic, proinflammatory molecule under development as an immunological adjuvant in vaccine formulations. Taking inspiration from the minimal length of assembly forming OES B segments in diblock copolymers, linear BAB and multiarm AB_4 copolymers form pseudocovalent shear-thinning gels with stability profiles mirroring their colloidal analogues. With facile control over PEG-OES copolymer block size and topology in this family of materials, we establish a role for very short ethylene sulfide oligomers in formation of supramolecular assemblies with user-defined morphology, oxidation-mediated disassembly, molecular loading and delivery capabilities, and robust aqueous stability.

RESULTS AND DISCUSSION

With a strategy of monomer-by-monomer adjustment of ethylene sulfide oligomer length, we prepared a family of highly asymmetric, AB-type PEG-OES diblock copolymer amphiphiles, the general structure of which is shown in Figure 2a. In our approach, monomethoxy-PEG-thioacetate molecules of two molecular weights were utilized as macroinitiator species for ring-opening anionic polymerization of ethylene sulfide (Supporting Information Figure S1). Chain length control and narrow dispersity are hallmarks of anionic polymerization of episulfides[35] such as ethylene sulfide, and the approach permits exquisite control over ethylene sulfide degree of polymerization, as confirmed by ^{1}H NMR spectroscopy (Figure 2b). Representative gel permeation chromatography resolved subtle differences in copolymer molecular weight (Supporting Information Figure S2). We performed systematic and stepwise extension of ethylene sulfide oligomer length until irreversible *in situ* precipitation

during chain growth; precipitates of copolymers 44-9 (PEG_{44}-*b*-OES_9) and 112-10 (PEG_{112}-*b*-OES_{10}) could not be resuspended in common solvents. As such, degrees of ethylene sulfide polymerization at and beyond these values were not explored in this study. At lower degrees of ethylene sulfide polymerization, the morphological behavior of PEG-OES diblock copolymer self-assemblies was defined by single-monomer differences in OES length (Figure 2c). Our purpose in OES length control was threefold: (1) to determine the smallest block size permitting assembly formation, (2) to characterize oligomer length control of assembly morphology, and (3) to identify morphological transition points, if any.

PEG-OES diblock copolymers subjected to a simple solvent evaporation technique generated spherical micellar and linear fibrillar colloidal self-assemblies, in which assembly formation and morphology depended on OES length, and therefore, mass fraction (f_{ES}) (Figure 2c,d; Supporting Information Figure S3 and S4). OES trimers represented the minimal block size required to form assemblies: self-assembly of PEG-OES diblock copolymer 44-3 yielded fibrillar constructs, whereas copolymer 44-2 failed to form assemblies. Copolymer 112-3 generated spherical micelles, and increasing OES length within the 112 family of polymers recapitulated formation of uniformly fibrillar populations with PEG-OES copolymer 112-9. Together these outcomes highlight strict dependence of assembly architecture on ethylene sulfide content; in both families, the threshold for fibril formation occurs at $f_{ES} \sim 0.08$ (Figure 2c). The influence of mass fraction on polymer-based self-assembly morphology has been exemplified in canonical studies of PEG-*b*-poly(1,2-butadiene).[12] Compared to amorphous PEG-*b*-poly(1,2-butadiene), in which no assembly structures were observed below poly(1,2-butadiene) mass fraction $f_{BD} \sim 0.28$, PEG-OES produces colloidal assemblies at much lower values for the mass fraction of the hydrophobic, assembly forming OES block, presumably due to its crystallinity. To demonstrate this crystallinity, we synthesized an OES homooligomer with degree of polymerization equal to three, and analyzed this material by differential scanning calorimetry. Analysis revealed a broad OES_3 melting transition centered around 118 °C, with no evidence of either glass or crystallization transitions (Supporting Information Figure S5); such a profile is characteristic of a crystalline polymeric material.

The diameters of the PEG-OES colloidal assemblies ranged from 12.7 to 25.7 nm and roughly scaled with increasing copolymer molecular weight (Figure 2c). Fibril-forming constituent polymers yielded high aspect ratio assemblies in which fibril lengths varied from hundreds of nanometers to several microns. In other crystallization-driven self-assembly systems, adjusting the length of the core-forming crystalline block has been shown to facilitate length control over rodlike cylindrical micelles.[36] In our group of fibril-forming PEG-OES diblock copolymers, the range of accessible ethylene sulfide oligomer lengths is considerably narrower, due to solubility constraints during polymer preparation. Although it was not possible to tune fibril dimensions during assembly formation, our fibrillar structures demonstrate considerably extended lengths when compared to truncated rodlike species such as those just described.

With the finding that ethylene sulfide-containing copolymers yield structural polymorphism in colloidal self-assemblies, we have expanded the family of materials in which polysulfide blocks drive assembly. Previously, our group utilized diblock and triblock copolymers of PEG and poly(propylene sulfide) (PPS) to prepare spherical micelles and vesicular polymersomes,[13,37] and these platforms have been explored as biomaterials in a variety of molecular delivery applications.[38−40] Due to the amorphous nature of the poly(propylene sulfide) hydrophobe ($T_g \sim 230$ K),[41] and its good solubility in common organic solvents, considerably longer PPS blocks may be accessed during ring-opening anionic polymerization of the monomer, on the order of tens of mers. However, to assemble PEG-PPS copolymer amphiphiles via hydrophobic interactions, these extended block lengths are essential. In contrast, we have shown that considerably shorter ethylene sulfide oligomers drive PEG-OES copolymer self-assembly, thanks to the crystalline nature of the OES domain. While the parameters for generating spherical micelles and vesicles are well-established for PPS-containing copolymers, wormlike micelle structures have only been accessed under limited conditions: as intermediate products of polymersome oxidation,[31] and as metastable assemblies prepared via thin film hydration.[13] In the present system, assembly via solvent evaporation method generated very stable spherical micelles as well as high aspect ratio linear fibrils.

With an interest in future biological applications of fibrillar assemblies, we explored both their aqueous stability and their stimulus-responsive behavior. As oligosulfide-containing materials, the fibril constructs are designed such that sulfide oxidation yields increasingly hydrophilic and amorphous sulfoxide and sulfone groups. These phenomena were monitored over time during incubation of 44-3 fibrils in 1% hydrogen peroxide. Copolymer 44-3 contains the shortest fibril-forming OES segment; these fibrils are therefore most susceptible to environmental oxidative conditions. Ongoing oxidation was defined by progressive decrease in ^{1}H NMR signal integration from protons adjacent to unmodified, unoxidized sulfide moieties, with concomitant increase in broad signals associated with protons in an oxidized environment (Figure 3a). Peak broadness reflected nonstatistical heterogeneous

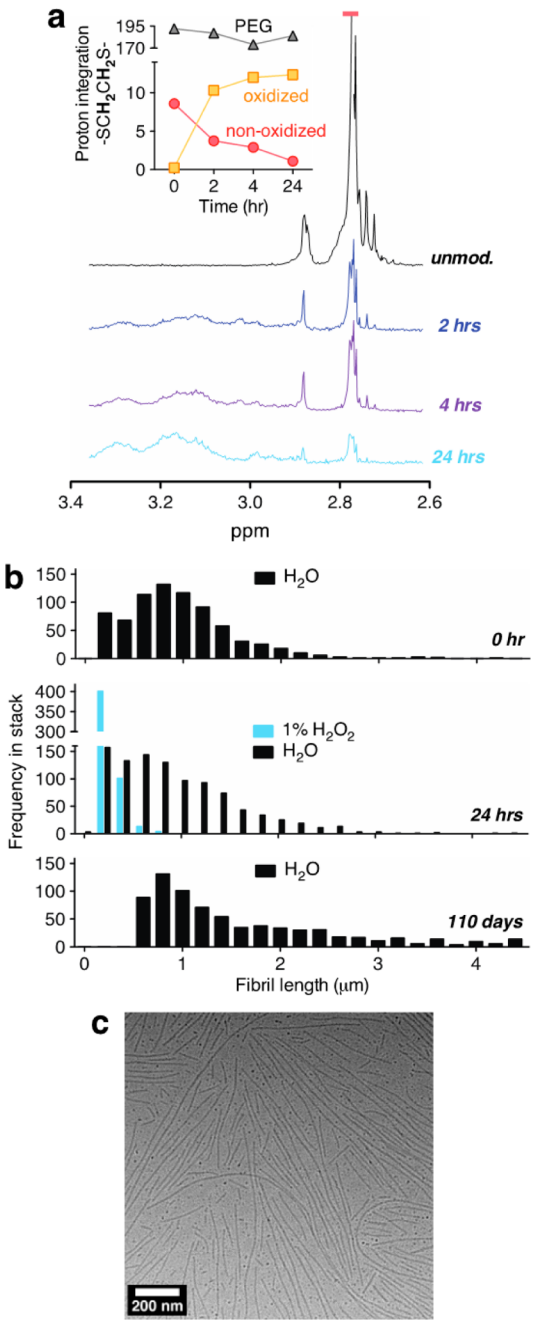

Figure 3. Ethylene sulfide oxidation promotes fibril shortening. (a) ^{1}H NMR spectroscopic analysis shows progressive and heterogeneous oxidation within the ethylene sulfide block during ongoing 1% hydrogen peroxide treatment of 44-3 fibrils (0−24 h). Decreasing signal integration of protons associated with nonoxidized sulfides (red circles) correlates with increasing signal integration of protons associated with oxidized sulfur species (yellow squares). (b) Oxidation decreases hydrophobicity and crystallinity of the OES block, promoting fibril shortening. In contrast, no change in fibril length is observed upon long-term storage in water. See also Supporting Information Figure S7 for a description of fibril image acquisition and quantitative image processing. (c) Fibril shortening and micelle formation after 24 h treatment with 1% hydrogen peroxide.

OES oxidation within the population of assembly forming polymers, which results from oxidative processes that occur in the context of a highly ordered assembly environment. The signal integration (Figure 3a, inset) and peak structure of PEG-associated protons were unchanged at all time points examined, confirming that oxidation under these conditions affects the OES block alone.

Oxidative processes drove progressive loss of copolymer amphiphilic behavior, the cumulative effects of which destabilize the assembly, promoting fibril shortening and formation of spherical micelles with greater interfacial curvature. In the absence of oxidation, fibrillar assemblies showed remarkable stability in water. Freshly prepared 44-3 fibrils in water varied from hundreds of nanometers to several microns in length (Figure 3b, top panel). This length distribution was unchanged after 24 h incubation in water at high dilution, whereas fibrils treated with 1% hydrogen peroxide underwent a significant shift in length distribution, favoring lower aspect ratio species (Figure 3b, middle panel). These morphological changes were confirmed by cryogenic transmission electron microscopy (cryoTEM), identifying shortened flexible fibrils and rodlike structures, as well as spherical micelles not observed in confocal microscopy imaging due to their subthreshold dimensions (Figure 3c). In cryoTEM imaging of 44-3 fibrils treated with 10% hydrogen peroxide for 24 h, the absence of defined structures correlated with complete oxidation-mediated disassembly to unimolecular species (image not shown). Without oxidation, fibrils retained their characteristic length distributions even following 110 days in water at high dilution (Figure 3b, bottom panel), highlighting the exceptional stability and storage capacity of aqueous fibril dispersions.

Complementary to our examination of fibril aqueous stability and oxidation-mediated disassembly, we undertook loading and *in vitro* delivery of a biologically relevant target molecule. MPLA is an immunostimulatory derivative of lipopolysaccharide that acts as an exogeneous danger signal to dendritic cells, promoting their activation and maturation. MPLA loading into 44-5 fibrils was achieved during the fibril formation process and did not interfere with assembly of the predicted high aspect ratio morphology (Supporting Information Figure S6). We subsequently examined the dose-dependent capacity of MPLA-loaded 44-5 fibrils to activate murine bone marrow-derived dendritic cells (BMDC). Following 20 h incubation with unloaded 44-5 fibrils, MPLA-loaded 44-5 fibrils, or free MPLA, BMDC activation was assessed by flow cytometric analysis of costimulatory molecules CD80 and CD86. These BMDC surface markers of activation were significantly upregulated following treatment with free MPLA and MPLA-loaded 44-5 fibrils at three different concentrations (Figure 4). As expected, treatment with unloaded 44-5 fibrils had no effect. These outcomes highlight the functional capacity of PEG-OES fibrils in small molecule

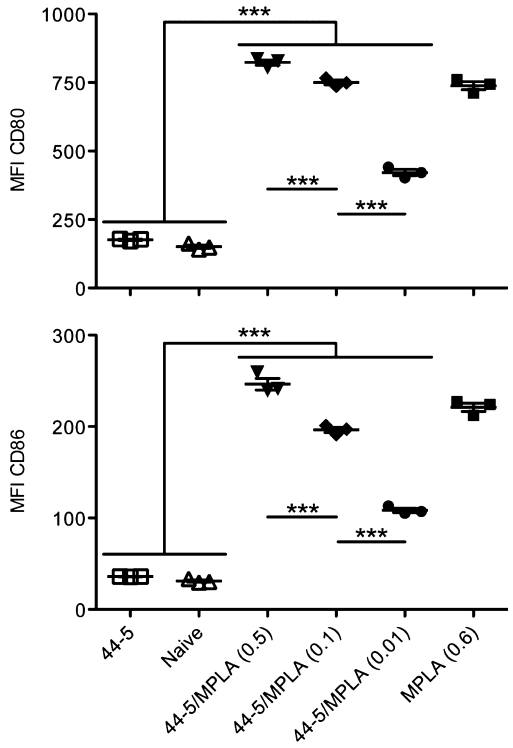

Figure 4. Dose-dependent dendritic cell activation by MPLA-loaded 44-5 fibrils. The mean fluorescence intensity (MFI) of bone marrow-derived dendritic cell activation markers CD80 (top panel) and CD86 (bottom panel) is significantly increased following incubation with MPLA-loaded 44-5 fibrils (44-5/MPLA) for 20 h. Values in parentheses represent total MPLA-derived endotoxin units (EU) per well as determined by TLR4 activation assay in HEK-Blue hTLR4 cells. Activation with free MPLA provides positive reference. ***$p < 0.0001$, for each of three 44-5/MPLA treatments compared to both unloaded 44-5 and naive treatments, and among 44-5/MPLA treatments. Statistical relationships to free MPLA have been omitted for clarity.

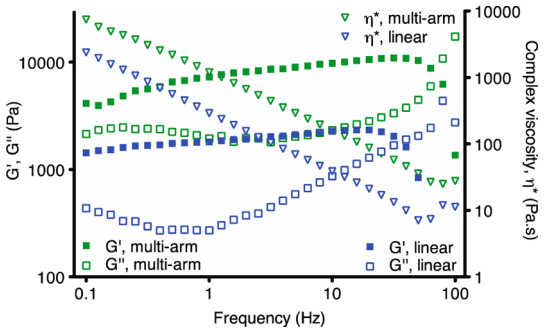

Figure 5. Oscillatory rheometry of physical hydrogels composed of linear (BAB) or multiarm (AB_4) precursors. Storage modulus (G'), loss modulus (G''), and complex viscosity (η^*) are frequency-dependent parameters in these shear-thinning hydrogels.

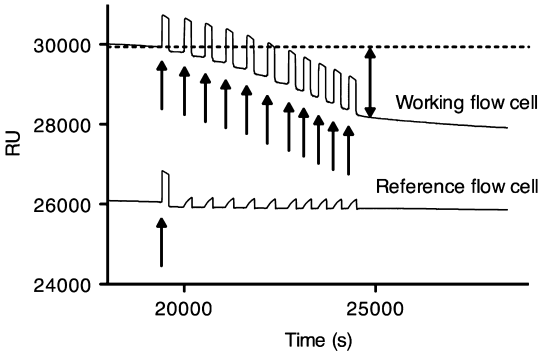

Figure 6. Surface plasmon resonance analysis of oxidation-mediated degradation in AB_4 physical hydrogel. Single-headed black arrows define initiation of a single 180 s 1% hydrogen peroxide injection event. The difference in pre-treatment and post-treatment signal baseline (double-headed black arrow) corresponds to decreased gel thickness due to mass loss in the working flow cell. Following one hydrogen peroxide injection event, continuous exposure to deionized water mobile phase does not impact gel thickness in the reference flow cell.

delivery, and further optimization of amphiphilic small molecule loading is presently underway.

Motivated by the colloidal assembly forming capability of very short ethylene sulfide oligomers, we predicted that OES crystallization would similarly drive network formation and physical gelation of linear triblock and multiarm precursors. Ring-opening oligomerization of ethylene sulfide from multifunctional PEG macroinitiators yielded linear BAB and multiarm AB_4 copolymers in which A represents the PEG domain and B represents tri(ethylene sulfide) (Figure 1). Applying the same solvent evaporation method used to prepare colloidal self-assemblies, we obtained solid gels from BAB and AB_4 precursors. In this technique, crystallization of OES trimers in both precursor types generated physical cross-links for supramolecular gel formation. Oscillatory mode rheological analysis of formed gels demonstrated storage and loss moduli similar to covalently cross-linked PEG diacrylate gels at low frequencies.[42] However, at higher frequencies, frequency-dependent changes in storage and loss moduli confirmed shear-thinning behavior, and the inverse linear dependence of complex viscosity on frequency underscored the solid-to-liquid transition in both gels (Figure 5). These physical gels therefore behave as pseudocovalent PEG-like hydrogels capable of distinct mechanical deformation.

Further stimulus-responsive behavior of physically cross-linked multiarm gels was elucidated in surface plasmon resonance analysis of gel erosion (Figure 6). In this technique, regions of gel-coated gold film defined as the reference or working flow cell were exposed to a deionized water mobile phase or 1% hydrogen peroxide. Changes in flow cell signal output reflect the dependence of gold's surface plasmon resonance angle on changes in gel thickness. Following a single hydrogen peroxide injection event to confirm proper flow conditions, continuous exposure to deionized water mobile phase yielded no change in reference flow cell signal baseline. It should be noted that signal disruptions resulting from hydrogen peroxide injection events in the working flow cell caused only transient

baseline distortions in the reference flow cell. In the working flow cell, repeated hydrogen peroxide injections accumulated decreasing signal output. Decreased signal output compared to pretreatment equilibrium conditions corresponded to decreased gel thickness resulting from gel mass loss. These changes represented oxidation-mediated mass loss of approximately 1700 pg/mm^2. This surface plasmon resonance analysis of physical gel networks confirmed observations from stability studies in colloidal fibril constructs: very short ethylene sulfide oligomers drive formation of supramolecular materials demonstrating excellent aqueous stability in combination with oxidation-dependent structural destabilization.

CONCLUSION

Here we have revisited the preparation of ethylene sulfide-containing block copolymer materials and established their new role in supramolecular assemblies. PEG-OES copolymer amphiphiles were synthesized with very precise length control in the assembly forming OES segment, thereby governing assembly structural morphology. Facile modulation of spherical (isotropic) versus fibrillar (anisotropic) structure is a valuable platform characteristic, given for example that colloidal architecture is now recognized to impact particle interaction with cells and tissues. The PEG-OES copolymers are entirely organic and do not contain iron-chelating species utilized in many crystalline-core cylindrical micellar assemblies.[24] Along with decreased toxicity and stealth behavior conferred by PEG content,[43] these characteristics support exploration of the colloidal and network assemblies in biological applications. Such potential utility is further emphasized by the robust aqueous stability of colloidal fibrillar dispersions and multiarm physical gels. MPLA-loaded fibril assemblies showed dose-dependent dendritic cell activation, demonstrating their potential for molecular delivery in biological systems. Susceptibility to oxidation-mediated disassembly imparts a biologically relevant, stimulus-responsive behavior and inherent degradation mechanism to these materials. Examining mechanical and chemical stimulus-responsive behavior in PEG-OES physical gels, we established interesting functional parameters of these materials. These efforts define a family of novel materials in which minimal-length self-assembling segments control a logical sequence of supramolecular assembly parameters, directing their formation, their morphology, and their disassembly.

METHODS

Preparation of PEG-Based Macroinitiator Species. Using linear poly(ethylene glycol) (PEG, MW 4600), linear monomethoxy-PEG (MW 2000 or 5000), or 4-arm PEG (MW 20,000) as the starting material, preparation of PEG-based macroinitiator species for ring opening polymerization was adapted from previously described methods for thioacetate modification of PEG terminal hydroxyl groups.[39,44]

Preparation of AB-Type PEG-OES Diblock Copolymers. Monomethoxy-PEG-thioacetate (mPEG-TA) was transferred to Schlenk tube under argon and dissolved in tetrahydrofuran (THF). The solution was stirred at room temperature under argon for 30 min following addition of sodium methoxide (0.5 M solution in methanol, 1.1 equiv). After sodium methoxide activation, various equivalents of ethylene sulfide monomer were added. The ring-opening oligomerization reaction was terminated with excess glacial acetic acid (Supporting Information Figure S1). Block copolymer product was obtained with 80−90% yield after washing, filtration, precipitation in diethyl ether, and vacuum drying. ^{1}H NMR spectroscopy was performed in $CDCl_3$ on the Bruker AVANCE (400 MHz) platform with Topspin software: δ = 3.83−3.44 (s, broad, OC**H$_2$**C**H$_2$**), 3.37 (s, OC**H$_3$**), 2.87 (m, C**H$_2$**SH) 2.85−2.76 (m, SC**H$_2$**C**H$_2$**), 2.74 (td, C**H$_2$**CH$_2$SH).

Preparation of OES$_3$ Homooligomer. β-Mercaptoethanol (BME, 0.040 mL, 1 equiv) was added to Schlenk tube containing THF under argon. The solution was stirred at room temperature under argon for 15 min following addition of sodium methoxide (0.5 M solution in methanol, 1.1 equiv). Addition of ethylene sulfide monomer (3 equiv) yielded tri(ethylene sulfide) oligomer growth from the thiolated BME initiator. Oligomerization was accompanied by *in situ* evolution of disperse, white, powdery precipitate. The reaction was terminated with excess glacial acetic acid. The precipitate product was obtained in 32% yield following THF and ether wash and vacuum drying. The homooligomer precipitate represented an intractable material resistant to all common organic solvents. Continuous 2 h sonication at 40 °C was required to achieve a sparing solubility in deuterated dimethyl sulfoxide sufficient for analysis. ^{1}H NMR spectroscopy (d_6-DMSO): δ = 3.53 (dd, HOC**H$_2$**), 2.93 (dd, C**H$_2$**SH), 2.74 (s, SC**H$_2$**C**H$_2$**), 2.68 (m, C**H$_2$**CH$_2$SH), 2.60 (t, HOCH$_2$C**H$_2$**).

Preparation of BAB-Type OES$_3$-PEG$_{104}$-OES$_3$ Triblock Copolymer. TA-PEG(4600)-TA macroinitiator was transferred to Schlenk tube under argon and dissolved in THF. The solution was stirred at room temperature under argon for 30 min following addition of sodium methoxide (0.5 M solution in methanol, 2.2 equiv). Addition of ethylene sulfide monomer (6 equiv) yielded simultaneous chain growth of tri(ethylene sulfide) oligomers from both macroinitiator termini. The reaction was terminated with excess glacial acetic acid. Polymer product was obtained in 87% yield after washing, filtration, diethyl ether precipitation, and vacuum drying. ^{1}H NMR spectroscopy ($CDCl_3$): δ = 3.83−3.44 (s, broad, OC**H$_2$**C**H$_2$**), 2.88 (m, C**H$_2$**SH), 2.85−2.76 (m, SC**H$_2$**C**H$_2$**), 2.74 (td, C**H$_2$**CH$_2$SH).

Preparation of AB$_4$-Type 4-Arm PEG(20,000)-(OES$_3$)$_4$ Block Copolymer. 4-Arm PEG(20,000)-(TA)$_4$ macroinitiator was transferred to Schlenk tube under argon and dissolved in THF with transient gentle heat. The solution was stirred at room temperature under argon for 30 min following addition of sodium methoxide (0.5 M solution in methanol, 4.4 equiv). Addition of ethylene sulfide monomer (12 equiv) yielded simultaneous chain growth of tri(ethylene sulfide) oligomers from each macroinitiator terminus. The reaction was terminated with excess glacial acetic acid. 4-arm PEG(20,000)-(OES$_3$H)$_4$ was obtained in 78% yield after washing, filtration, diethyl ether precipitation, and vacuum drying. ^{1}H NMR spectroscopy ($CDCl_3$): δ = 3.83−3.44 (s, broad, OC**H$_2$**C**H$_2$**), 2.87 (m, C**H$_2$**SH), 2.85−2.76 (m, SC**H$_2$**C**H$_2$**), 2.74 (td, C**H$_2$**CH$_2$SH).

Preparation of Colloidal Assemblies. Spherical micelles and linear fibrils were generated by solvent evaporation technique. AB-type PEG-OES diblock copolymers were dissolved in THF (1 w/v%), with gentle stirring. For preparation of fluorescent assemblies, lipophilic dye DiO was added at a final concentration of 5 μM. Subsequently, deionized water was added at a volume equivalent to that of THF. The reaction was stirred under

ambient conditions until complete THF evaporation. In the absence of DiO labeling, all resulting aqueous colloidal dispersions were clear and colorless. Dispersions containing DiO-labeled assemblies were clear and faintly yellow; these samples underwent exhaustive diafiltration against deionized water (MWCO 3,000) to remove unincorporated dye molecules. For preparation of MPLA-loaded fibrils, PEG-OES diblock copolymer 44−5 was dissolved in THF (1 w/v%). MPLA (Monophosphoryl Lipid A from *S. minnesota* R595, InvivoGen; 500 μg/mL in 10:90 dimethyl sulfoxide/phosphate-buffered saline) was added (0.8 mol % of 44-5 content), followed by a volume of deionized water equivalent to that of THF. The reaction was stirred under ambient conditions until complete THF evaporation. Trace DMSO was removed by diafiltration against deionized water (MWCO 3000). Subsequently, unincorporated MPLA was removed by diafiltration against 50:50 deionized water: methanol (MWCO 30 000) to yield MPLA-loaded 44-5 fibril dispersions.

Transmission Electron Microscopy (TEM). For negative stain TEM, 5 μL of colloidal sample solution was adsorbed to a glow-discharged carbon-coated copper grid (Canemco & Marivac), washed with deionized water, and stained with 2% uranyl acetate. The samples were imaged at room temperature using a Tecnai Spirit electron microscope equipped with LaB6 filament and operated at an acceleration voltage of 80 kV. Images were obtained at 30 000−50 000× magnification. For cryo-TEM, 4−5 μL colloidal sample solution was applied to electron microscopy grid (Agar Scientific) with holey carbon film. Sample grids were blotted and flash vitrified in liquid ethane using an automatic plunge freezing apparatus (Vitrobot, FEI) to control humidity (100%) and temperature (23 °C). Analysis was performed at −170 °C on a Tecnai F20 electron microscope operating at 200 kV, using the Gatan 626 cryo-specimen holder (20 000−50 000× magnification; −3 to −5 μm defocus). Digital images were recorded on in-line Eagle CCD camera, and assembly diameters were measured using the Fiji (version 1.48) distribution[45] of ImageJ.[46]

Confocal Microscopy. To suspend Brownian motion in aqueous dispersions, fluorescent colloidal assemblies were fixed in *bis*-acrylamide cross-linked polyacrylamide gel (5%). Several microliters assembly containing gel were immobilized between glass slide and slide cover immediately prior to visualization. Confocal microscopy was performed on a Leica TCS SP5 laser scanning confocal microscope with 63× 1.4 NA oil immersion objective, using acquisition software Leica LAS AF 2009. Embedded DiO-labeled assemblies were excited with a 488 nm Argon laser at 30% power and detected over a wavelength range of 492−550 nm with a HyD detector at 100% detector gain, 1000 hz scanning speed, line averaging of 4, 1024 × 1024 resolution, and zoom factor of 6. The resulting three-dimensional confocal image stacks had 20 nm *x*−*y* resolution and 210 nm *z* resolution covering a volume of 41 μm (width) × 41 μm (height) × 5 μm (depth). Images stacks were processed with the Fiji (version 1.48) distribution[45] of ImageJ[46] (Supporting Information Figure S7). Raw image stacks were preprocessed for quantification utilizing the ImageJ deconvolution lab plugin[47] followed by binary thresholding and noise filtration with built-in ImageJ functions. The processed image stacks were quantified with the 3D-objects counter plugin.[48]

Oxidation of Fibrillar Assemblies. Fibrillar assemblies composed of diblock copolymer PEG_{44}-OES_3 (polymer 44-3) were exposed to 1% or 10% hydrogen peroxide in water for 24 h. At several time points, samples were removed and exhaustively diafiltered (MWCO 3000) against deionized water, prior to analysis by NMR spectroscopy and cryogenic transmission electron microscopy. Oxidized samples were freeze-dried to disrupt remaining assemblies and resuspended in $CDCl_3$ for NMR spectroscopic analysis.

***In Vitro* Dendritic Cell Activation Assay.** C57BL/6J mice (7−8 weeks) were purchased from Harlan Laboratories and housed under pathogen-free conditions at the animal facility of Ecole Polytechnique Fédérale de Lausanne. All experiments were performed in accordance with Swiss law and with approval from the Cantonal Veterinary Office of Canton de Vaud, Switzerland. Bone marrow-derived dendritic cells (BMDC) were harvested from mouse bone marrow and cultured for 8 days prior to use, as described elsewhere.[49] BMDC were incubated for 20 h in RPMI medium or RPMI medium containing unloaded 44-5 fibrils (500 μg/mL) or free MPLA (2.5 μg/mL) or MPLA-loaded 44-5 fibrils (500, 50, or 5 μg/mL). Endotoxin levels of BMDC treatment formulations were quantified with InvivoGen HEK-Blue hTLR4 cell system using LPS standard. BMDC maturation markers CD80 and CD86 were analyzed by flow cytometry in $CD11c^+$ $MHCII^+$ populations. CD80 and CD86 mean fluorescence intensity values were analyzed by one-way ANOVA followed by Tukey's multiple comparisons post-test.

Gel Formation and Analysis. Here, 20% physical gels of OES_3-PEG_{104}-OES_3 (BAB-type) or 4-arm PEG(20,000)-$(OES_3)_4$ (AB_4-type) were formed by dissolving the polymer precursors in THF, adding an equivalent volume of deionized water, and removing volatile THF. Rheological analysis was performed at 22 °C on a stress-controlled TA Instrument AR 2000ex rheometer with Rheology Advantage software package, using 20 mm cone and plate geometry. Frequency dependence of storage modulus, loss modulus, and complex viscosity was analyzed in oscillatory mode with 1% applied strain. Surface plasmon resonance was carried out on a BIAcore X100 platform (GE Healthcare) using deionized water as the mobile phase at 30 μL/min systemic flow. Immediately prior to analysis, a 20 w/v% solution of PEG(20,000)-$(OES_3H)_4$ in THF was spin-coated onto purpose-made gold-coated SPR wafers (BIAcore) and vacuum-dried. Rehydration yielded an adherent gel film. Following system equilibration, the reference flow cell was once exposed (180 s) to 1% hydrogen peroxide in water and the working flow cell was repeatedly exposed in 180 s bursts to 1% hydrogen peroxide in water. Mass loss from the working flow cell correlates to signal loss compared to pretreatment equilibrium baseline signal.

Conflict of Interest: The authors declare no competing financial interest.

Acknowledgment. This work was supported by ERC Advanced Grant NanoImmune, under the Seventh Framework Programme (J.A.H) and by the Whitaker Foundation/IIE (C.E.B). We gratefully recognize F. Spiga for technical assistance with SPR acquisition, and F. Sordo and T. Nardi for rheometer access. ^{1}H NMR spectroscopy was performed in the EPFL Institute of Chemical Sciences and Engineering. The EPFL Molecular and Hybrid Materials Characterization Center and J. Morisod are recognized for DSC access and training. Confocal microscopy was acquired in the EPFL BioImaging and Optics Platform. We thank C. Card and D. S. Wilson for editorial feedback during manuscript preparation.

Supporting Information Available: PEG-OES synthetic scheme, gel permeation chromatography, additional cryoTEM imaging, dynamic light scattering, differential scanning calorimetry, and an overview of confocal microscopy image processing for fibril length scale analysis. The Supporting Information is available free of charge on the ACS Publications website at DOI: 10.1021/acsnano.5b02937.

REFERENCES AND NOTES

1. Zhulina, E. B.; Adam, M.; LaRue, I.; Sheiko, S. S.; Rubinstein, M. Diblock Copolymer Micelles in a Dilute Solution. *Macromolecules* **2005**, *38*, 5330–5351.
2. Bates, F. S.; Hillmyer, M. A.; Lodge, T. P.; Bates, C. M.; Delaney, K. T.; Fredrickson, G. H. Multiblock Polymers: Panacea or Pandora's Box? *Science* **2012**, *336*, 434–440.
3. Elsabahy, M.; Wooley, K. L. Design of Polymeric Nanoparticles for Biomedical Delivery Applications. *Chem. Soc. Rev.* **2012**, *41*, 2545–2561.
4. Aida, T.; Meijer, E. W.; Stupp, S. I. Functional Supramolecular Polymers. *Science* **2012**, *335*, 813–817.
5. Hudalla, G. A.; Modica, J. A.; Tian, Y. F.; Rudra, J. S.; Chong, A. S.; Sun, T.; Mrksich, M.; Collier, J. H. A Self-Adjuvanting Supramolecular Vaccine Carrying a Folded Protein Antigen. *Adv. Healthcare Mater.* **2013**, *2*, 1114–1119.
6. Loverde, S. M.; Klein, M. L.; Discher, D. E. Nanoparticle Shape Improves Delivery: Rational Coarse Grain Molecular

Dynamics (RCG-MD) of Taxol in Worm-Like PEG-PCL Micelles. *Adv. Mater.* **2012**, *24*, 3823–3830.
7. Geng, Y.; Dalhaimer, P.; Cai, S.; Tsai, R.; Tewari, M.; Minko, T.; Discher, D. E. Shape Effects of Filaments *Versus* Spherical Particles in Flow and Drug Delivery. *Nat. Nanotechnol.* **2007**, *2*, 249–255.
8. Shi, X.; von dem Bussche, A.; Hurt, R. H.; Kane, A. B.; Gao, H. Cell Entry of One-Dimensional Nanomaterials Occurs by Tip Recognition and Rotation. *Nat. Nanotechnol.* **2011**, *6*, 714–719.
9. Kolhar, P.; Anselmo, A. C.; Gupta, V.; Pant, K.; Prabhakarpandian, B.; Ruoslahti, E.; Mitragotri, S. Using Shape Effects to Target Antibody-Coated Nanoparticles to Lung and Brain Endothelium. *Proc. Natl. Acad. Sci. U. S. A.* **2013**, *110*, 10753–10758.
10. Albertazzi, L.; van der Zwaag, D.; Leenders, C. M. A.; Fitzner, R.; van der Hofstad, R. W.; Meijer, E. W. Probing Exchange Pathways in One-Dimensional Aggregates with Super-Resolution Microscopy. *Science* **2014**, *344*, 491–495.
11. Ortony, J. H.; Newcomb, C. J.; Matson, J. B.; Palmer, L. C.; Doan, P. E.; Hoffman, B. M.; Stupp, S. I. Internal Dynamics of a Supramolecular Nanofibre. *Nat. Mater.* **2014**, *13*, 812–816.
12. Jain, S.; Bates, F. S. On the Origins of Morphological Complexity in Block Copolymer Surfactants. *Science* **2003**, *300*, 460–464.
13. Cerritelli, S.; O'Neil, C. P.; Velluto, D.; Fontana, A.; Adrian, M.; Dubochet, J.; Hubbell, J. A. Aggregation Behavior of Poly(Ethylene Glycol-bl-Propylene Sulfide) Di- and Triblock Copolymers in Aqueous Solution. *Langmuir* **2009**, *25*, 11328–11335.
14. Warren, N. J.; Mykhaylyk, O. O.; Mahmood, D.; Ryan, A. J.; Armes, S. P. Raft Aqueous Dispersion Polymerization Yields Poly(Ethylene Glycol)-Based Diblock Copolymer Nano-Objects with Predictable Single Phase Morphologies. *J. Am. Chem. Soc.* **2014**, *136*, 1023–1033.
15. Chen, S.; Cheng, S. X.; Zhuo, R. X. Self-Assembly Strategy for the Preparation of Polymer-Based Nanoparticles for Drug and Gene Delivery. *Macromol. Biosci.* **2011**, *11*, 576–589.
16. Li, S.-L.; Xiao, T.; Lin, C.; Wang, L. Advanced Supramolecular Polymers Constructed by Orthogonal Self-Assembly. *Chem. Soc. Rev.* **2012**, *41*, 5950–5968.
17. Wang, X.; Guerin, G.; Wang, H.; Wang, Y.; Manners, I.; Winnik, M. A. Cylindrical Block Copolymer Micelles and Co-Micelles of Controlled Length and Architecture. *Science* **2007**, *317*, 644–647.
18. Gadt, T.; Ieong, N. S.; Cambridge, G.; Winnik, M. A.; Manners, I. Complex and Hierarchical Micelle Architectures from Diblock Copolymers Using Living, Crystallization-Driven Polymerizations. *Nat. Mater.* **2009**, *8*, 144–150.
19. Hsiao, M.-S.; Yusoff, S. F. M.; Winnik, M. A.; Manners, I. Crystallization-Driven Self-Assembly of Block Copolymers with a Short Crystallizable Core-Forming Segment: Controlling Micelle Morphology through the Influence of Molar Mass and Solvent Selectivity. *Macromolecules* **2014**, *47*, 2361–2372.
20. Du, Z.-X.; Xu, J.-T.; Fan, Z.-Q. Micellar Morphologies of Poly(e-Caprolactone)-b-Poly(Ethylene Oxide) Block Copolymers in Water with a Crystalline Core. *Macromolecules* **2007**, *40*, 7633–7637.
21. Petzetakis, N.; Walker, D.; Dove, A. P.; O'Reilly, R. K. Crystallization-Driven Sphere-to-Rod Transition of Poly(Lactide)-b-Poly(Acrylic Acid) Diblock Copolymers: Mechanism and Kinetics. *Soft Matter* **2012**, *8*, 7408–7414.
22. Li, Z.; Liu, R.; Mai, B.; Wang, W.; Wu, Q.; Liang, G.; Gao, H.; Zhu, F. Temperature-Induced and Crystallization-Driven Self-Assembly of Polyethylene-b-Poly(Ethylene Oxide) in Solution. *Polymer* **2013**, *54*, 1663–1670.
23. Mihut, A. M.; Crassous, J. J.; Schmalz, H.; Drechsler, M.; Ballauff, M. Self-Assembly of Crystalline-Coil Diblock Copolymers in Solution: Experimental Phase Map. *Soft Matter* **2012**, *8*, 3163–3173.
24. Schmelz, J.; Schacher, F. H.; Schmalz, H. Cylindrical Crystalline-Core Micelles: Pushing the Limits of Solution Self-Assembly. *Soft Matter* **2013**, *9*, 2101–2107.
25. Takahashi, Y.; Tadokoro, H.; Chatani, Y. Structure of Polyethylene Sulfide. *J. Macromol. Sci., Part B: Phys.* **1968**, *2*, 361–367.
26. Moss, B.; Dorset, D. L. Poly(Ethylene Sulfide): Reevaluation of the Electron Diffraction Structure Analysis. *J. Macromol. Sci., Part B: Phys.* **1983**, *22*, 69–77.
27. Cooper, W.; Hale, P. T.; Walker, J. S. Elastomeric Block Polymers from Ethylene Sulfide. *Polymer* **1974**, *15*, 175–186.
28. Pal, A.; Karthikeyan, S.; Sijbesma, R. P. Coexisting Hydrophobic Compartments through Self-Sorting in Rod-Like Micelles of Bisurea Bolaamphiphiles. *J. Am. Chem. Soc.* **2010**, *132*, 7842–7843.
29. Pawar, G. M.; Koenigs, M.; Fahimi, Z.; Cox, M.; Voets, I. K.; Wyss, H. M.; Sijbesma, R. P. Injectable Hydrogels from Segmented PEG-Bisurea Copolymers. *Biomacromolecules* **2012**, *13*, 3966–3976.
30. Lee, S. H.; Gupta, M. K.; Bang, J. B.; Bae, H.; Sung, H. J. Current Progress in Reactive Oxygen Species (ROS)-Responsive Materials for Biomedical Applications. *Adv. Healthcare Mater.* **2013**, *2*, 908–915.
31. Napoli, A.; Valentini, M.; Tirelli, N.; Muller, M.; Hubbell, J. A. Oxidation-Responsive Polymeric Vesicles. *Nat. Mater.* **2004**, *3*, 183–189.
32. Han, P.; Ma, N.; Ren, H.; Xu, H.; Li, Z.; Wang, Z.; Zhang, X. Oxidation-Responsive Micelles Based on a Selenium-Containing Polymeric Superamphiphile. *Langmuir* **2010**, *26*, 14414–14418.
33. Wang, X.-J.; Xing, L.-B.; Wang, F.; Wang, G.-X.; Chen, B.; Tung, C.-H.; Wu, L.-Z. Multistimuli Responsive Micelles Formed by a Tetrathiafulvalene-Functionalized Amphiphile. *Langmuir* **2011**, *27*, 8665–8671.
34. Bertrand, N.; Leroux, J.-C. The Journey of a Drug-Carrier in the Body: An Anatomo-Physiological Perspective. *J. Controlled Release* **2012**, *161*, 152–163.
35. Vo, C. D.; Kilcher, G.; Tirelli, N. Polymers and Sulfur: What Are Organic Polysulfides Good For? Preparative Strategies and Biological Applications. *Macromol. Rapid Commun.* **2009**, *30*, 299–315.
36. Sun, L.; Petzetakis, N.; Pitto-Barry, A.; Schiller, T. L.; Kirby, N.; Keddie, D. J.; Boyd, B. J.; O'Reilly, R. K.; Dove, A. P. Tuning the Size of Cylindrical Micelles from Poly(L-Lactide)-b-Poly(Acrylic Acid) Diblock Copolymers Based on Crystallization-Driven Self-Assembly. *Macromolecules* **2013**, *46*, 9074–9082.
37. Napoli, A.; Tirelli, N.; Wehrli, E.; Hubbell, J. A. Lyotropic Behavior in Water of Amphiphilic ABA Triblock Copolymers Based on Poly(Propylene Sulfide) and Poly(Ethylene Glycol). *Langmuir* **2002**, *18*, 8324–8329.
38. Segura, T.; Hubbell, J. A. Synthesis and *In Vitro* Characterization of an ABC Triblock Copolymer for siRNA Delivery. *Bioconjugate Chem.* **2007**, *18*, 736–745.
39. Velluto, D.; Demurtas, D.; Hubbell, J. A. PEG-b-PPS Diblock Copolymer Aggregates for Hydrophobic Drug Solubilization and Release: Cyclosporin A as an Example. *Mol. Pharmaceutics* **2008**, *5*, 632–642.
40. Scott, E. A.; Stano, A.; Gillard, M.; Maio-Liu, A. C.; Swartz, M. A.; Hubbell, J. A. Dendritic Cell Activation and T Cell Priming with Adjuvant- and Antigen-Loaded Oxidation-Sensitive Polymersomes. *Biomaterials* **2012**, *33*, 6211–6219.
41. Nicol, E.; Nicolai, T.; Durand, D. Dynamics of Poly(Propylene Sulfide) Studied by Dynamic Mechanical Measurements and Dielectric Spectroscopy. *Macromolecules* **1999**, *32*, 7530–7536.
42. Patel, P. N.; Smith, C. K.; Patrick, C. W. Rheological and Recovery Properties of Poly(Ethylene Glycol) Diacrylate Hydrogels and Human Adipose Tissue. *J. Biomed. Mater. Res., Part A* **2005**, *73A*, 313–319.
43. Otsuka, H.; Nagasaki, Y.; Kataoka, K. PEGylated Nanoparticles for Biological and Pharmaceutical Applications. *Adv. Drug Delivery Rev.* **2003**, *55*, 403–419.
44. Napoli, A.; Tirelli, N.; Kilcher, G.; Hubbell, J. A. New Synthetic Methodologies for Amphiphilic Multiblock Copolymers of Ethylene Glycol and Propylene Sulfide. *Macromolecules* **2001**, *34*, 8913–8917.

45. Schindelin, J.; Arganda-Carreras, I.; Frise, E.; Kaynig, V.; Longair, M.; Pietzsch, T.; Preibisch, S.; Rueden, C.; Saalfeld, S.; Schmid, B.; et al. Fiji: An Open-Source Platform for Biological-Image Analysis. *Nat. Methods* **2012**, *9*, 676–682.
46. Schneider, C. A.; Rasband, W. S.; Eliceiri, K. W. NIH Image to ImageJ: 25 Years of Image Analysis. *Nat. Methods* **2012**, *9*, 671–675.
47. Vonesch, C.; Unser, M. A Fast Thresholded Landweber Algorithm for Wavelet-Regularized Multidimensional Deconvolution. *IEEE Trans. Image Process.* **2008**, *17*, 539–549.
48. Bolte, S.; Cordelieres, F. P. A Guided Tour into Subcellular Colocalization Analysis in Light Microscopy. *J. Microsc.* **2006**, *224*, 213–232.
49. Lutz, M. B.; Kukutsch, N.; Ogilvie, A. L.; Rossner, S.; Koch, F.; Romani, N.; Schuler, G. An Advanced Culture Method for Generating Large Quantities of Highly Pure Dendritic Cells from Mouse Bone Marrow. *J. Immunol. Methods* **1999**, *223*, 77–92.